PHYSICAL REVIEW C VOLUME 25, NUMBER 2 FEBRUARY 1982

Recoil and correlations in pion double scattering

D. M. Schneider, M. K. Banerjee, J. W. Van Orden, and S. J. Wallace
Department of Physics and Astronomy, University of Maryland, College Park, Maryland 20742
(Received 19 February 1981)

The contribution to the optical potential due to double scattering of a pion by a pair of correlated nucleons has been calculated for nuclear matter taking account of nucleon and delta kinetic energies. The calculation includes a variety of field theoretical effects due to crossed processes and all possible time sequences of the two scattering events including overlap in time. For sequential processes, where the first scattering is complete before the second starts, it is found that inclusion of kinetic energies of the nucleon and delta reduces the contribution drastically. The contribution of these sequential processes is about 2% of the first-order optical potential as contrasted with about 50% at $T_\pi = 140$ MeV when the fixed scatterer approximation is employed. The most important correlated double scattering contributions arise from the field theoretical effects which yield about 8% of the first-order optical potential at $T_\pi = 0$ and 140 MeV. Thus, the net contribution of correlated double scattering processes is about 10% of the first-order optical potential. Since the double scattering of the pion by a correlated nucleon pair is a major contributor to the Ericson-Ericson effect, the present work suggests reduced importance of the effect.

[NUCLEAR REACTIONS Correlations, fixed scatterer approximation, LLEE effect, double scattering, recoil, pion scattering.]

I. INTRODUCTION

In this paper, we calculate the optical potential contribution due to double scattering of a pion from a correlated pair of nucleons in the nucleus. A logical separation is made between scattering processes and pion absorption processes, each of which forms a major component of the second-order pion-nuclear optical potential. Absorption by correlated nucleon pairs is the subject of a future paper.

The contribution to the optical potential due to correlated double scattering has its own independent history as exemplified by recent work[1] and older work bearing on the so-called Lorentz-Lorenz Ericson-Ericson (LLEE) effect.[2] The history of pion double scattering is dominated by calculations based on the fixed scatterer approximation (FSA).[3] In FSA, the amplitude for the pion to scatter from two fixed nucleons is averaged over a static correlation density to get the final amplitude.

The πN interaction is strongest in the P wave and the off-mass-shell P wave scattering amplitude increases with increasing pion momenta over a large range of momenta. As a result of this and the fact that nucleon-nucleon correlations can support high momentum, the pion tends to have high momentum in its flight between the two nucleons. Conservation of momentum requires that during the flight of the pion the nucleon struck first must recoil with correspondingly high momentum. This has two consequences. First, the energy of recoil of the struck nucleons must be taken into account. Second, since the intermediate states have, of necessity, high energy, other processes involving comparable energy must also be considered. An example would be crossed processes where a pion is emitted before it is absorbed. Another example is a situation where the two scattering amplitudes overlap in time. These processes are possible because the pion number need not be conserved. A nucleon can become a delta not only by absorbing a pion but also by emitting one. Such events will be referred to as field theoretical effects.

Treatments using FSA usually include only those double scattering processes where interaction one ends before interaction two begins (in time). We refer to these as sequential processes and the corresponding diagrams as sequential diagrams. These are the only processes describable by multiple scattering theory based on a πN potential. Field theoretical effects usually are not included in treatments using FSA.

As the object of the paper is only to assess the

importance of ground state correlation in double scattering, all calculations have been done for nuclear matter. There are several additional simplifying approximations which are described in Sec. III.

Calculations based on FSA produce very large second-order optical potentials, ranging from $\sim 16\%$ of the first-order optical potential at pion laboratory energy $T_\pi = 0$ to $\sim 50\%$ at $T_\pi = 140$ MeV. Eisenberg *et al.*[4] pointed out that the contribution of double scattering may be much smaller if the πN form factor is sufficiently soft. Recent work[5] on the πN P-wave interaction has shown that the form factor is quite hard. Thus, the expected reduction does not occur. We find that upon inclusion of recoil the contribution of the sequential processes reduces to less than 2% of the first-order optical potential at both energies. However, when field theoretical effects are included, the second-order optical potential increases to $\sim 10\%$ of the first-order optical at both $T_\pi = 0$ and 140 MeV.

In a recent paper[6] we have described a new organization of π-nuclear scattering based on a Goldstone expression of the π-nuclear optical potential. The organization centers on the construction of a self-consistent πN t matrix in the nuclear medium. This is done in a manner which emphasizes the importance of the effects of the medium on the πN (elastic) intermediate states of the πN t matrix in the nucleus. A set of diagrammatic elements is required to represent the driving term of the self-consistent equation. Not only do these diagrammatic elements provide a first estimate of the optical potential, but also serve as building blocks to generate all other possible diagrammatic contributions to the optical potential through the self-consistent equation. These diagrammatic elements consist of two classes. First, all diagrams contributing to the free πN t matrix with appropriate modifications for Pauli blocking and binding shifts are included in the set of diagrammatic elements. Second, the remaining diagrams in the set of diagrammatic elements contain nucleon-nucleon correlations and do not contain πN (elastic) intermediate states where there are any elastic interactions of the π with the nuclear medium. In the previous paper only diagrammatic elements from the first class were used in order to make the calculation tractable. Clearly, the next logical step is to consider the contribution to the optical potential of the leading order diagrams of the second class containing ground state correlations as is done in this paper and in a subsequent paper studying the absorption of a π on a correlated NN pair.

II. CLASSIFICATION OF DIAGRAMS

In this section we list and classify the Goldstone diagrams one must evaluate to obtain the optical potential contribution due to pion double scattering by a correlated nucleon pair. The rules for Goldstone diagrams for pion-nuclear processes have appeared elsewhere.[7,1] In the Appendix we give the standard rules and an additional rule for the off-shell N interactions which arise in pion-nuclear processes.

Altogether, 144 diagrams are considered. Let us begin with two particularly simple diagrams, namely the sequential diagrams of Fig. 1, where Fig. 1(b) is obtained from Fig. 1(a) upon interchanging the hole lines. In these diagrams the off-shell πN scattering is indicated by a cross hatched box and the nucleon-nucleon G matrix is represented by the horizontal wavy lines. Upward directed solid lines represent particles and downward directed lines represent holes. We will always consider diagrams in such direct-exchange pairs as in Figs. 1(a) and 1(b), which ensures the antisymmetry of the two-nucleon states. Therefore, it suffices to discuss only half of the 144 diagrams with the understanding that the remaining 72 diagrams, obtained by exchanging hole lines, are present and are taken into account.

Accompanying the sequential process of Fig. 1(a) is a set of five diagrams shown in Fig. 2, which represent the other possible time orderings of the two scattering events. The diagrams of Fig. 2 represent field theoretical effects. Note that on the left-hand side, the beginning and the end of the πN interaction (hatched box) is accompanied by absorption of a pion. On the right-hand side a

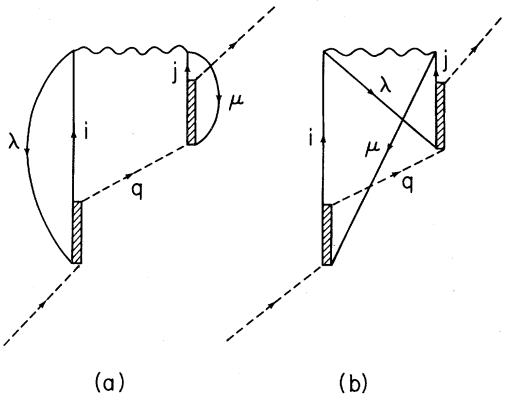

FIG. 1. A double scattering diagram and its exchange.

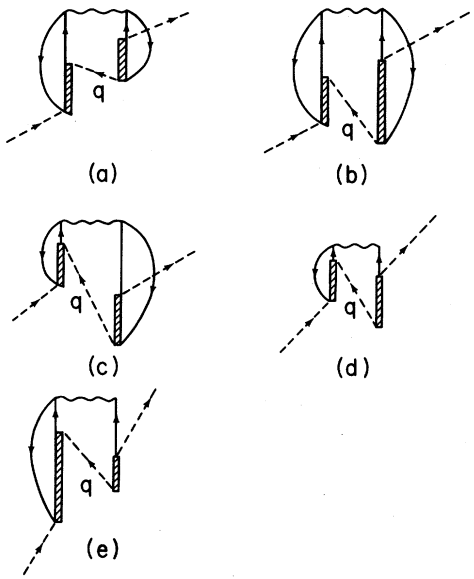

FIG. 2. Diagrams obtained from Fig. 1(a) by time ordering the endpoints of the deltas (cross-hatched box).

pion is emitted at both ends. Figure 1(a) will be termed as diagram 1. Figures 2(a)–2(d) will be termed as diagrams 2–6.

For every diagram of this set of six there are three more obtained by crossing the two pion lines at the end of each hatched box. Figures 3–5 are the crossed counterparts obtained from Fig. 1(a). When all possible time orderings are included, the diagram of Fig. 3 expands to a set of six diagrams and the same thing happens to the diagrams of Figs. 4 and 5. The set headed by Fig. 3 will be labeled diagrams 7–12, the set headed by Fig. 4 will be labeled diagrams 13–18, and finally, the set headed by Fig. 5 will be labeled diagrams 19–24. For convenience, the four sets of six diagrams will be referred to as sets 1–4 corresponding to the sequence in which they were introduced. The diagrams in sets 2–4 follow the same sequence of time ordering of the two scattering events as those in set 1.

These 24 diagrams together with the 24 exchange diagrams complete the list of all double scattering diagrams in which the nuclear G matrix appears after the end of the two-pion scattering processes. We call these prescattering processes. For every prescattering event there is a postscattering counterpart. Figure 6(b) shows the postscatter-

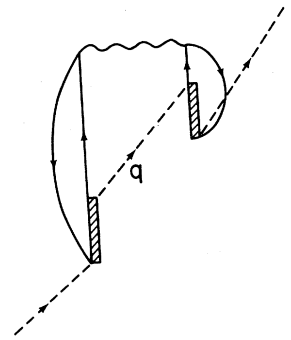

FIG. 4. Diagram obtained from Fig. 1(a) by interchanging the entrance and exit points on the second delta. To this diagram there corresponds five more obtained by the time orderings of the endpoints of the deltas.

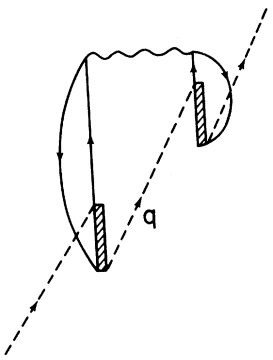

FIG. 3. Diagrams obtained from Fig. 1(a) by interchanging the entrance and exit points of the pion lines on both deltas. To this diagram there corresponds five more obtained by the time orderings of the endpoints of the deltas.

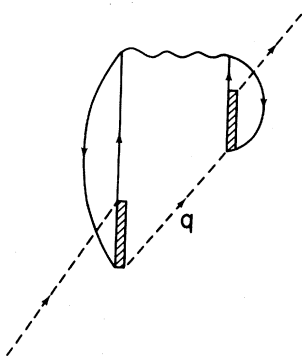

FIG. 5. Diagram obtained from Fig. 3(a) by interchanging the entrance and exit points on the first delta. To this diagram there corresponds five more obtained by the time orderings of the endpoints of the deltas.

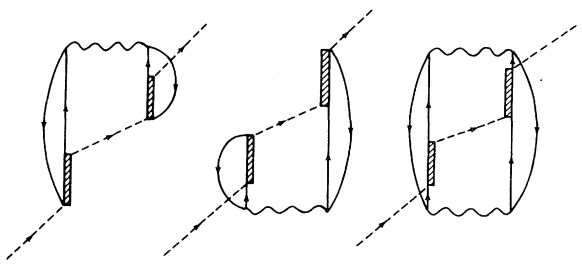

FIG. 6. (a) A prescattering event which is the same as Fig. 1(a). (b) The corresponding postscattering event. (c) The intermediate scattering event.

ing counterpart of Fig. 6(a) which is diagram 1. Figure 6(c) shows the intermediate scattering counterpart of diagram 1. Here the scattering events are sandwiched between two G matrices. This completes the listing of the 144 diagrams mentioned earlier.

III. SEQUENTIAL PROCESSES

As stated at the outset, our calculations are for nuclear matter. We make several further approximations, described below, all designed to facilitate the calculation without affecting the usefulness of the qualitative conclusions.

(a) The Fermi motion of the nucleon is ignored. All hole energies are replaced with an average value $-B=-21$ MeV.

(b) We include only the $P33$ channel for the πN t matrix. The static projection operator for this channel is used as given in Eq. (A2) of the Appendix.

(c) We use the nonrelativistic form for kinetic energies of the nucleon and delta.

(d) The integrations over internal pion momenta are cut off at $10m_\pi$. This simple choice is based on the recent result[6] that the $P33$ form factor varies very slowly for small momenta [see Eq. (A1) of the Appendix].

(e) We also regard the external pion momentum to be small compared to the typical momentum of the internal pion. This momentum is set to zero everywhere except in the $P33$ projection operators.

(f) For sequential processes, we need only the off-shell πN amplitude $h_R(x)$ obtained from the right-hand cut of the full πN amplitude:

$$h_R(x-\epsilon^\Delta)=\frac{1}{\pi}\int\frac{h_{33}(z)dz}{z-x+\epsilon^\Delta-i\eta}\ , \tag{1a}$$

where $h_{33}(z)$ is the on-shell function appearing in the expression for the t matrix,

$$t_{\alpha\beta}(\omega,k,k')=\sum_{I,J}^{1/2,3/2}h_{2I,2J}(\omega)P_{2I,2J}(\alpha,\beta,k,k') \tag{1b}$$

as is given by

$$h_{2I,2J}(\omega)=-\frac{(1/4\pi)(W/M)\eta_{2I,2J}(\omega)e^{2i\delta_{2I,2J}}-1}{2iq^3}\ . \tag{1c}$$

The phase shifts are given in the center of mass, hence, the appearance of the recoil energy ϵ^Δ in the argument of h_R accounts, in an approximate way, for the c.m. to laboratory transformation.

Using the Goldstone rules and Eq. (1) one obtains for diagram 1 and its hole line exchange counterpart

$$U_1=\int\frac{d^3\vec{q}}{(2\pi)^3 2\omega_q}\sum_\beta\sum_{\substack{ij>k_F\\ \lambda\mu<k_F}}[(\lambda\mu\,|\,G\,|\,ij)-(\mu\lambda\,|\,G\,|\,ij)]\frac{1}{\epsilon_\lambda+\epsilon_\mu-\epsilon_i-\epsilon_j}$$
$$\times h_R(\omega+\epsilon_\mu+\epsilon_\lambda-\epsilon_i-\epsilon_j-\epsilon_q^\Delta)\langle j\,|\,P_{33}(\beta,\alpha,\vec{q},\vec{k})\,|\,\mu\rangle\frac{1}{\omega+\epsilon_\lambda-\epsilon_i-\omega_q+i\eta}$$
$$\times h_R(\omega-\epsilon_k^\Delta+\epsilon_\lambda)\langle i\,|\,P_{33}(\alpha,\beta,\vec{k},\vec{q})\,|\,\lambda\rangle\ . \tag{2}$$

Here, i,j label the particle states and λ,μ label the hole states of the nucleon. ϵ_i, etc., are the energies of these single-particle states. The quantities ϵ_q^Δ and ϵ_k^Δ are defined as

$$\epsilon_q^\Delta=\frac{q^2}{2M_\Delta}$$

and

$$\epsilon_k^{\Delta}=\frac{k^2}{2M_{\Delta}} . \tag{3}$$

With approximation (e) it follows that the particle state i has momentum $-\vec{q}$, the state j has momentum $\vec{q}$ and $\epsilon_k^{\Delta}\approx 0$. We set

$$\epsilon_i=\epsilon_j=\frac{q^2}{2M} . \tag{4}$$

Consistent with approximation (a) we ignore Pauli blocking. Thus, the range of q is from $0m_{\pi}$ to $10m_{\pi}$. The defect function[8]

$$\chi_{\lambda\mu}(ij)=-\frac{(\lambda\mu \mid G \mid ij)-(\mu\lambda \mid G \mid ij)}{\epsilon_{\lambda}+\epsilon_{\mu}-\epsilon_i-\epsilon_j} \tag{5}$$

is related to the Bethe-Goldstone correlated wave function ψ through $\psi=\phi-\chi$, where ϕ is the unperturbed product wave function. Incorporating the various simplifying approximation one gets

$$U_1=-(\tfrac{1}{4}\rho)^2\int\frac{d^3\vec{q}}{(2\pi)^3 2\omega_q}\,\mathrm{Tr}\sum_{\beta}\chi(\vec{q})h_R\left[\omega-2B-\frac{q^2}{2M}-\frac{q^2}{2M_{\Delta}}\right]P_{33}^{(2)}(\beta,\alpha,\vec{q},\vec{k})$$

$$\times h_R(\omega-B)P_{33}^{(1)}(\alpha,\beta,\vec{k},\vec{q})[\omega-B-q^2/(2M)-\omega_q+i\eta]^{-1} . \tag{6}$$

Here, $\rho=2k_F^3/3\pi^2$ is the nuclear matter density. We take $k_F=1.9m_{\pi}$. The symbol Tr means the spin and isospin traces for both nucleons. The channel projection operators are operators in single nucleon spin-isospin space. The superscripts are the nucleon labels. The relative motion defect function is also an operator in the spin-isospin space of the two nucleons. It may be written in the following form:

$$\chi(\vec{q})=4\pi[\chi(q,{}^1S)\Omega_s\Lambda_t+\chi(q,{}^3S)\Omega_t\Lambda_s+\chi(q,{}^3S\rightarrow{}^3D)\Omega_{SD}\Lambda_s] , \tag{7}$$

where it has been decomposed into its singlet S, triplet S, and triplet D components. These are all for a starting S-wave relative motion. Ω_s,Ω_t are the S-wave singlet and triplet projection operators given by

$$\Omega_s=\tfrac{1}{4}(1-\vec{\sigma}_1\cdot\vec{\sigma}_2) ,$$
$$\Omega_t=\tfrac{1}{4}(3+\vec{\sigma}_1\cdot\vec{\sigma}_2) , \tag{8a}$$

with the analogous singlet and triplet isospin operators given by

$$\Lambda_s=\tfrac{1}{4}(1-\vec{\tau}_1\cdot\vec{\tau}_2) ,$$
$$\Lambda_t=\tfrac{1}{4}(3+\vec{\tau}_1\cdot\vec{\tau}_2) . \tag{8b}$$

We also have Ω_{SD}, which operating on the triplet $S_{J=1}$ spin angular momentum state produces a triplet $D_{J=1}$ state

$$\Omega_{SD}=\frac{3\vec{q}\cdot\vec{\sigma}_1(\vec{q}\cdot\vec{\sigma}_2)-q^2\vec{\sigma}_1\cdot\vec{\sigma}_2}{\sqrt{8}} . \tag{8c}$$

The quantity $\chi(q,{}^1S)$ is the ${}^1S$ defect function in the momentum space. $\chi(q,{}^3S)$ and $\chi(q,{}^3S\rightarrow{}^3D)$ are the S and D defect functions with the unperturbed state being ${}^3S_1$. These defect functions were calculated with the Reid soft core B (Ref. 9) potential. Carrying out the spin-isospin traces one has

$$U_1=-k^2\rho^2 h_R(\omega-B)\frac{2}{\pi}\int\frac{q^4dq}{2\omega_q}\frac{h_R[\omega-2B(q^2/2M)-(q^2/2M_\Delta)]}{\omega-B-\omega_q-(q^2/2M)+i\eta}$$
$$\times\left[\tfrac{7}{54}\chi(q,{}^1S)+\tfrac{7}{54}\chi(q,{}^3S)-\frac{\sqrt{2}}{108}\chi(q,{}^3S\to{}^3D)\right]. \quad (9)$$

Inclusion of nucleon and Δ energies produces two effects. First and more important is the change in the effective pion energy in the second πN scattering amplitude. Instead of being equal to ω, the external pion energy, it is reduced by the excitation energy of the nucleon and delta. The factor q^4, appearing because of the P wave nature of the interaction, coupled with the ability of the defect functions to support high momentum causes most of the integral in Eq. (9) to come from large q values. The root mean square value of q in a typical defect function is about $4m_\pi$. Thus, the change in the effective pion energy is quite large and this recoil effect drastically reduces the value of h_R compared to $h_R(\omega)$, the value used in a FSA calculation. The second effect is the appearance of nucleon recoil energy in the denominator. While not as dramatic as the effect of recoil on the πN amplitude, it is not a negligible feature.

The expression given by Eq. (9) for the contribution of the sequential process of the prescattering class to the optical potential was evaluated at two values of pion laboratory energy T_π, viz., 0 and 140 MeV. The numerical results are shown in the first row of Table I. The second row of Table I gives the result of evaluating the sequential process in the static limit, i.e., when the nucleon and delta kinetic energies in Eq. (9) are dropped. One sees that inclusion of baryon kinetic energies results in a reduction of the contribution by a factor of 5 at $T_\pi=0$. For $T_\pi=140$ the reduction in the imaginary part is almost by a factor of 40.

It should be noted that the static limit of (9) does not produce the popular form of the FSA result for the prescattering (PS) process. The latter is

$$U_{\rm FSA}^{\rm PS}=-\tfrac{1}{3}k^2\rho^2[h_R(\omega)+h_R(-\omega)]^2\frac{2}{\pi}$$
$$\times\int\frac{q^4dq}{\omega^2-m_\pi{}^2-q^2+i\eta}\chi(q,S) \quad (10)$$

and it differs from the static limit of (9) in several respects. In FSA the full scattering amplitude is used for both scattering events. We have indicated this by adding the left-hand cut and then squaring, since omission of the nucleon pole terms is of little consequence in the present context. In the static limit the denominator of (9) is $2\omega_q(\omega-\omega_q)$. In FSA this is replaced with the nonrelativistic form $\vec{k}_0{}^2-\vec{q}^2$, where $k_0{}^2=\omega^2-m_\pi{}^2$, which is then used for the entire range of $\vec{q}$. Finally, in the FSA it is not customary to pay close attention to the details of the spin-isospin algebra. The defect function $\chi(q,S)$ is some suitable defect function for the relative S state. As we will see later, we need the value of the defect function at zero internucleon separation and this value is independent of spin. Writing

$$\frac{q^2}{\omega^2-m_\pi{}^2-q^2+i\eta}=-1+\frac{\omega^2-m_\pi{}^2}{\omega^2-m_\pi{}^2-q^2+i\eta},$$

we once again drop the pole term on the right-

TABLE I. Contributions to the optical potential. The numbers are in units of $10^{-2}k^2/m_\pi{}^3$.

	$T_\pi=0$	$T_\pi=140$ MeV
Sequential diagram (1) (prescattering)	0.755	$2.67+i1.63$
Sequential diagram with no recoil (prescattering)	3.95	$-9.5+i63.4$
FSA [Eq. (15)]	16.37	$-58.2+i123.0$
First-order optical potential	-93.5	$-144.0-i228.0$

hand side for reasons to be discussed shortly. One gets

$$U_{\mathrm{PSA}}^{PS}=\tfrac{1}{3}k^2\rho^2[h_R(\omega)+h_R(-\omega)]^2\frac{2}{\pi}\int q^2dq\,\chi(q)\ . \tag{11}$$

For future convenience we cast (11) in the form of a matrix of an operator Λ_{FSA} between the defect function χ and the unperturbed wave function ϕ,

$$U_{\mathrm{FSA}}^{\mathrm{PS}}=-\langle\chi\,|\,\Lambda_{\mathrm{FSA}}\,|\,\phi\rangle\ , \tag{12}$$

with

$$\Lambda_{\mathrm{FSA}}=-\tfrac{1}{3}k^2\rho^2[h_R(\omega)+h_R(-\omega)]^2\delta(\vec{\mathrm{r}})\ . \tag{13}$$

In terms of Λ_{FSA} the postscattering contribution is $\langle\phi\,|\,\Lambda_{\mathrm{FSA}}\,|\,\chi\rangle$ and the intermediate scattering contribution is $-\langle\chi\,|\,\Lambda_{\mathrm{FSA}}\,|\,\chi\rangle$. The total is

$$\begin{aligned}U_{\mathrm{FSA}}&=-\langle\chi|\Lambda_{\mathrm{FSA}}|\phi\rangle-\langle\phi|\,\Lambda_{\mathrm{FSA}}|\,\chi\rangle+\langle\chi|\,\Lambda_{\mathrm{FSA}}|\,\chi\rangle\\&=\langle\psi\,|\,\Lambda_{\mathrm{FSA}}\,|\,\psi\rangle-\langle\phi\,|\,\Lambda_{\mathrm{FSA}}\,|\,\phi\rangle\ ,\end{aligned} \tag{14}$$

where ψ is the Bethe-Goldstone wave function. Since Λ_{FSA} contains $\delta(\vec{\mathrm{r}})$ one gets

$$U_{\mathrm{FSA}}=+\tfrac{1}{3}k^2\rho^2[h_R(\omega)+h_R(-\omega)]^2\ , \tag{15}$$

where we have used $\phi(\vec{\mathrm{r}}=0)=1$ and $\psi(\vec{\mathrm{r}}=0)\approx 0$, the latter because of the strong short range repulsion between nucleons. Note that the full FSA result is identically equal to $U_{\mathrm{FSA}}^{\mathrm{PS}}$.

The form (14) is true for every triad of postscattering, prescattering, and intermediate scattering diagrams 1–24. The sum of all 144 diagrams can be represented as

$$U=\sum_{n=1}^{24}(\langle\psi\,|\,\Lambda_n\,|\,\psi\rangle-\langle\phi\,|\,\Lambda_n\,|\,\phi\rangle)\ ,$$

where Λ_n is a two-nucleon operator appropriate for the nth diagram. Whenever the pion propagator has a pole, whether in FSA or for any of the 24 diagrams, Λ will have an infinite range part $\sim e^{iq_Pr}/r$, where q_P is the position of the pole in the variable q, and r is the internucleon distance. Since the Bethe-Goldstone wave function ψ rapidly heals up to the unperturbed wave function $\phi(r)$ the infinite range part of Λ contributes little to the second-order optical potential.

The third row of Table I contains values obtained from Eq. (15). The last row of Table I contains the values of the first-order optical potential, which is

$$U^{(0)}=\tfrac{4}{3}k^2\rho[h_R(\omega-B)+h_R(-\omega-B)]\ . \tag{16}$$

The factor $\frac{4}{3}$ comes from spin-isospin averaging of the $P33$ projection operator. An examination of the results for $T_\pi=140$ MeV immediately shows the need to take the recoil energies into account. Both static calculations give contributions whose imaginary parts are $\frac{1}{4}$ to $\frac{1}{2}$ of that of the first-order optical potential. While the calculation taking account of the recoil energies gives an imaginary contribution less than 2% of the imaginary part of the first-order potential.

Because the sequential processes are suppressed so strongly by the recoil effects it becomes necessary to examine the contribution of the field theoretical effects described by the remaining diagrams. This is done in the next section.

IV. ALL PRESCATTERING DIAGRAMS

In this section we consider all prescattering diagrams. Half of these diagrams are obtained from the other half by interchanging the entry and exit points of the external pion, i.e., by crossing.[10] For example, set 2 can be obtained from set 1 by crossing and the last three diagrams of set 3 (diagrams 16–18) are the crossed counterparts of the first three (diagrams 13–15). Similarly, in set 4, the last three diagrams are the crossed counterparts of the first three. In the present calculation the external pion momenta, which are equal, appear only in the external factor $\vec{\mathrm{k}}^2$. The initial and final isospins are also the same. So the only result of crossing is to change the sign of ω, the external pion energy. Thus, it suffices to consider half of the terms and evaluate them at both positive ω and negative ω.

Evaluation of any diagram requires a three-dimensional integration over $\vec{\mathrm{q}}$ and integration over the mass variables z_1 and z_2 associated with the left and the right hatched boxes, respectively. The integrands of the six diagrams in any set differ from each other only in the four-denominator factor that appears. The denominator occurring immediately below the G matrix is the same for all diagrams. In the previous section we have seen how this denominator together with the G matrix gives the defect function. Let the symbol d_n stand for the product of the remaining three denominators of the nth diagram. The integrals over z_1 and z_2 are carried out most conveniently if the integrand can be arranged to have the following two features. First, no factor contains both z_1 and z_2. Second, z_1 and z_2 each appear in only one

denominator. Then, the integrals factorize, and the z_1 and z_2 integrations may be performed to give a product of two h_R amplitudes [see Eq. (10)]. But most d_n's are not of the desired form. Nevertheless, it is possible to arrange the integrands to have the desired feature by partial summation of groups of terms (generalized time ordering[8]) and occasionally decomposing a single product of denominators into a sum of products. These points are illustrated with the denominators of the first three diagrams, viz.,

$$d_1=\frac{1}{\omega-2B-(q^2/2M)-(q^2/2M_\Delta)-z_2}\,\frac{1}{\omega-B-(q^2/2M)-\omega_q}\,\frac{1}{\omega-B-z_1}\,, \tag{17a}$$

$$d_2=\frac{1}{\omega-2B-(q^2/2M)-(q^2/2M_\Delta)-z_2}\,\frac{1}{\omega-\omega_q-2B-(q^2/2M_\Delta)-z_1-z_2}\,\frac{1}{\omega-B-z_1}\,, \tag{17b}$$

$$d_3=\frac{1}{\omega-2B-(q^2/2M)-(q^2/2M_\Delta)-z_2}\,\frac{1}{\omega-\omega_q-2B-(q^2/2M_\Delta)-z_1-z_2}\,\frac{1}{-\omega_q-B-(q^2/2M_\Delta)-z_2}\,. \tag{17c}$$

While d_1 is of the desired form, d_2 and d_3 are not. Summing the two we get

$$d_2+d_3=\frac{1}{\omega-2B-(q^2/2M)-(q^2/2M_\Delta)-z_2}\,\frac{1}{-\omega_q-B-(q^2/2M_\Delta)-z_2}\,\frac{1}{\omega-B-z_1}\,,$$

which does not have any factor containing both z_1 and z_2 but still has two factors containing z_2. That is remedied by decomposition into partial fractions.

$$d_2+d_3=\frac{1}{\omega-B-z_1}\,\frac{1}{\omega-B-(q^2/2M)+\omega_q}\left[-\frac{1}{\omega-2B-(q^2/2M)-(q^2/2M_\Delta)-z_2}+\frac{1}{-\omega_q-B-(q^2/2M_\Delta)-z_2}\right]. \tag{18}$$

Now the two terms are both in the desired form. We note also that the first term of (18) differs from d_1, given by (17a) only in the sign of ω_q in the middle term. The sum of the two produces a Klein-Gordon–type denominator $[(\omega-B-q^2/2M)^2-\omega_q{}^2]^{-1}$. Finally, the sum of the six diagrams of set 1 is given:

$$\sum_n^{\text{set 1}} U_n=-k^2\rho^2\frac{2}{\pi}\int q^2dq\,F_1(q)\times\left\{h_R\left[\omega-\frac{q^2}{2M_\Delta}-\frac{q^2}{2M}-2B\right]\frac{1}{[\omega-(q^2/2M)-B]^2-\omega_q{}^2+i\eta}h_R(\omega-B)+h_R\left[-\omega_q-\frac{q^2}{2M_\Delta}-B\right]\frac{B+(q^2/2M)}{\omega_q}\,\frac{1}{(\omega+\omega_q)^2-(q^2/2M+B)^2+i\eta}h_R(\omega-B)\right\}, \tag{19}$$

where

$$F_1(q)=\tfrac{7}{54}[\chi(q,{}^1S)+\chi(q,{}^3S)]-\frac{\sqrt{2}}{108}\chi(q,{}^3S\to{}^3D)\,. \tag{20}$$

An examination of the arguments of the h_R functions shows that the first term in the curly bracket of (19) is the larger of the two. The second term involves h_R far from the positive energy resonance. The relevant part of Eq. (19) differs from the result for diagram 1, given by (9), in having the denominator $[2\omega_q(\omega-B-\omega_q-q^2/2M+i\eta]^{-1}$ replaced by the Klein-Gordon–type propagator. One expects this replacement to cause an increase by a factor of ~ 2 in the contribution to the optical potential. The result of

calculation is given in the first row of Table II and the expected increase occurs. Note that the tensor correlation contributes significantly. The expression for set 2 is obtained by replacing ω with $-\omega$ in Eq. (19). The effective pion energy, the argument of h_R, is negative for all four h_R's and consequently the contribution is very small as given in the second row of Table II. Note that the contribution is real. This is because of two reasons. First, the amplitudes h_R are all real, the arguments being less than m_π. Second, no pole term appears in the pion propagator when $\omega \to -\omega$. The result for set 3 is

$$\sum_n^{\text{set 3}} U_n = -k^2\rho^2 \frac{2}{\pi} \int q^4 dq\, F_2(q) \left\{ h_R(-\omega - B) \left[1 + \frac{B + (q^2/2M)}{\omega_q} \right] \frac{1}{\omega^2 - [\omega_q + (q^2/2M) + B]^2} h_R(\omega - B) \right\}, \tag{21}$$

where

$$F_2(q) = \tfrac{5}{18}\{ \chi(q, {}^1S) + \chi(q, {}^3S) \} + \frac{\sqrt{2}}{36} \chi(q, {}^3S \to {}^3D) . \tag{22}$$

These diagrams have different spin-isospin structure which results in $F_2(q)$ being different from $F_1(q)$. Had it not been for the tensor correlation, $F_2(q)$ would be $\frac{15}{7}$ times larger than $F_1(q)$. Since the set is by itself crossing symmetric the expression (21) is an even function of ω.

The most remarkable feature of (21) is in the effective pion energies at which the amplitudes h_R's are evaluated. They contain no nucleon or delta kinetic energies. The absence of the latter is easy to understand. The first delta is formed by the incoming pion, hence $\epsilon^\Delta = k^2/2M_\Delta \approx 0$ in our approximation scheme. The second delta formation is accompanied by the emission of the outgoing pion. So, once again $\epsilon^\Delta = k^2/2M_\Delta \approx 0$. The removal of all reference to the recoil energy of the nucleon is not obvious at all. The result appears only after summing the six diagrams. The sum is of the generalized time ordering type. Comparing (21) with the first part of (19) shows two major differences. The first is the replacement of $F_1(q)$ by $F_2(q)$, which has been mentioned already. The second is the effective energy appearing in the first h_R function. For set 1 the energy argument is $\omega - 2B - q^2/2M - q^2/2M_\Delta$, showing the reduction due to the kinetic energy of the nucleon and the delta. In (21) the energy is $-\omega - B$. In both cases, the h_R function is reduced considerably relative to the value of $h_R(\omega)$. The two reductions are, *a priori,* comparable. The reason why the contribution of set 3, given in row 3 of Table II, is consistently larger than that of set 1 is because[11] $F_2(q) > F_1(q)$. The diagrams of set 4 gives the following expression which is an even function of ω:

$$\begin{aligned} \sum_n^{\text{set 4}} U_n = -k^2\rho^2 \frac{2}{\pi} \int q^4 dq\, F_2(q) h_R \left[-\omega_q - B - \frac{q^2}{2M_\Delta} \right] \\ \times \left\{ h_R \left[\omega - 2B - \frac{q^2}{2M} - \frac{q^2}{2M_\Delta} \right] \frac{1}{[\omega - (q^2/2M) - B]^2 - {\omega_q}^2} \right. \\ + h_R \left[-\omega - 2B - \frac{q^2}{2M} - \frac{q^2}{2M_\Delta} \right] \frac{1}{[-\omega - (q^2/2M) - B]^2 - {\omega_q}^2} \\ \left. - h_R \left[-\omega_q - B - \frac{q^2}{2M} \right] \frac{1}{\omega^2 - [\omega_q - (q^2/2M) - B]^2} \left[1 - \frac{(q^2/2M) + B}{\omega_q} \right] \right\} . \end{aligned} \tag{23}$$

In every h_R function appearing in (23) the energy argument is considerably less than ω. Naturally, the contribution, given in row 4 of Table II, is small.

The study of the prescattering diagrams may be summarized as follows. Of the four sets only sets 1 and 3 are important. Set 1, which contains the sequential diagram, gives a contribution which is much smaller than the FSA value because of the recoil effects. Set 3, which gives the largest contribution, is purely field theoretical in origin. The sum of all postscattering diagrams is $\sim 6\%$ of the first-order potential at both values of T_π.

V. ALL DIAGRAMS

As remarked earlier the sum of all postscattering diagrams is identically equal to the sum of all pre-

TABLE II. Decomposition of the prescattering (Sec. IV) contributions to the optical potential. For each energy the partial contributions of ^1S, ^3S, and tensor correlations are listed. The last row gives the first-order optical potential. All numbers are in $10^{-2}k^2/m_\pi^3$.

	$T_\pi=0$				$T_\pi=140$ MeV			
	^1S	^3S	Tensor	Total	^1S	^3S	Tensor	Total
Set 1	0.60	0.75	0.24	1.58	$1.92+i0.26$	$1.26+i2.58$	$1.20+i1.90$	$4.38+i4.74$
Set 2	0.18	0.22	0.06	0.46	$0.18-i0.007$	$0.14+i0.002$	$0.08-i0.002$	$0.40-i0.007$
Set 3	1.82	2.06	−0.70	3.18	$2.74+i4.39$	$2.94+i5.62$	$-1.39-i2.38$	$4.29+i7.63$
Set 4	0.23	0.31	−0.16	0.38	$-0.026-i0.26$	$0.22+i0.02$	$-0.43+i0.04$	$-0.236-i0.27$
	Total prescattering			5.61	Total prescattering			$8.83+i12.25$
	FSA for prescattering			16.37	FSA for prescattering			$-58.20+i123.2$
	First-order			−93.51	First-order			$-144.30-i227.8$

scattering diagrams. In FSA the intermediate scattering [in the sense of Fig. 6(c)] gives a contribution equal in magnitude but opposite in sign to that of the postscattering or prescattering diagrams. The situation is radically altered when the nucleon kinetic energies are taken into account. From Fig. 6(c) it is clear that both πN scatterings takes place when there is considerable excitation present. In sets 1 and 3, $\omega-B$ appeared as the argument of one of the h_R functions. This does not happen in any of the intermediate scattering diagrams. Therefore, one expects the contribution to be quite small.

The evaluation of the 48 diagrams of the intermediate scattering type is somewhat tedious and considerably time consuming because the integrals for the delta mass variables do not factorize. We have done the calculation for $T_\pi=0$ only. At this energy, the pion propagators do not have poles and so no subtraction is necessary. This reduces the computational time. We obtain

$$\sum_{n=1}^{24} U_n(\text{intermediate scattering};\ T_\pi=0)$$
$$=-1.74\times10^{-2}\frac{k^2}{m_\pi^3}\ . \tag{24}$$

About 90% of the value comes from the s-wave correlations. The value given in (24) is about 30% of the contribution of the prescattering diagrams and ~2% of the first-order optical potential. As one approaches the resonance the relative contribution of the intermediate scattering contribution will be even smaller. The factor $h_R(\omega-B)$ appearing in the prescattering diagrams will increase, while none of the h_R functions appearing in the intermediate scattering diagrams will.

Taking 2% of the first-order optical potential as an estimate of the contribution of the intermediate scattering diagrams at $T_\pi=140$ MeV also we conclude that the full contribution of pion double scattering by a correlated nucleon pair is ~10% at both energies.

In view of the smallness of the double scattering contribution it is reasonable to expect that the contributions of triple and higher order pion scattering from correlated clusters will be negligible. To see this it is sufficient to note that energy arguments of the additional scattering amplitudes which occur in the evaluation of these higher order processes are either negative of order $\sim-\omega$, or considerably reduced from $+\omega$ because of subtraction of the energies of the excited nucleons.

VI. SUMMARY AND CONCLUSIONS

We find the FSA overestimates considerably the contribution of pion double scattering by a correlated nucleon pair to the pion-nucleus optical potential. When the kinetic energies of the nucleons and the deltas are taken into account the contribution of the sequential process is less than 2% of the first-order optical potential. The FSA estimate ranges from 25–50%. The large reduction is a consequence of the strong energy dependence of the πN t matrix element. Thought of another way, the reduction occurs because the πN interaction is sufficiently extended in time due to the 33 resonance to vitiate the static correlations between two nucleons. Because the first nucleon recoils during the resonant scattering with a second nucleon, the interparticle separation r_{12} tends to become large. The double scattering operator Λ (including recoil)

becomes long ranged, and thus, has a reduced overlap with the defect wave function χ. For this reason, previous static treatments of the role of ground state correlations in pion scattering come into serious doubt.

The πN t matrix consists very generally of two parts due to crossing symmetry, namely, the right- and left-hand contributions. In pion-nuclear scattering these two parts enter in quite different ways necessitating in the present paper a separation of the right- and left-hand cut contributions to $t_{\pi N}$. The rules for embedding the πN t matrix into pion-nuclear scattering have been given and the field theoretical processes have been dealt with in a systematic fashion. Because of the suppression of the sequential processes, the field theoretic effects gain in relative importance in correlated double scattering. When all the effects are counted in double scattering contribution to the optical potential is estimated to be $\sim 10\%$. Thus, the LLEE effect also will be correspondingly reduced.

ACKNOWLEDGMENTS

The support of the U. S. Department of Energy and the University of Maryland Computer Science Center is gratefully acknowledged. We wish to thank Mrs. Loretta Robinette for her assistance in the preparation of this paper. In addition, we thank G. A. Miller for a useful comment and William L. Truex for supplying us with the defect functions used for this work.

APPENDIX

We will draw diagrams for the pion-nucleus t matrix element. A Goldstone diagram consists of directed lines for pions, nucleons, and other particles and vertices where three or more of these lines join. If a potential theory for NN interaction is used there will be nondirected horizontal lines of specified character connecting two nucleon lines to indicate potential interactions.

The type of lines used in this paper are

(i) Dashed lines for pions;

(ii) Upward solid lines for nucleons in unoccupied (particle) states, downward lines for occupied (hole) states;

(iii) Horizontal wiggly lines represent G matrices. Single potential lines are never exhibited separately.

(iv) In this paper a thin, directed, rectangular, hatched box will represent an interacting πN system. These are employed as a device to describe the πN t matrix conveniently. It will facilitate the handling of the energy of the amplitude in the presence of excitation. This point is discussed later.

All of our diagrams will have two external lines, incoming and outgoing pion lines, for the sole purpose of visual convenience. No numerical factor, such as a denominator, is to be associated with these lines.

We list below six rules for evaluation of a Goldstone diagram.

(1) Associate to each internal line an appropriate set of quantum numbers (e.g., spin-isospin, momentum). The energy of the line is determined by the chosen Hamiltonian and the quantum numbers. The energy associated with the external line is the incoming energy ω.

(2) Between successive vertices there is an energy denominator. To determine this denominator we draw for each diagram an auxiliary diagram, where we remove the original external pion lines and then replace them with a single line directed from the exit point (last interaction point of external line) to the entry point (first interaction point). This line is directed upward or downward depending on the time ordering of the first and last interactions. A denominator is equal to the sum of energy of all downward-going lines minus the sum of all upward-going lines present in the interval.

(3) The rules for the vertices and G matrix interactions are the usual ones.

(4) Form the product of all denominators and matrix elements of interactions and sum over all internal variables.

(5) The sign of any contribution of any diagram is given by $(-1)^{h+l}$. h is the number of hole lines, and l is the number of closed Fermion loops.

These rules have to be supplemented by a sixth rule designed to handle situations where during the course of interaction of a pion with a nucleon, other events are occurring elsewhere in the medium. The rule becomes intuitively obvious upon reviewing the method of handling a πN t matrix (a four-point function) appearing as part of a larger Feynman graph. In order to do the energy loop integral it is convenient to write the t matrix as an analytic function of the sum of the energies of the entering

pion and nucleon lines. The role and treatment of the nucleon poles, direct and crossed, are obvious and need no elaboration. The right- and left-hand cuts are handled by moving the interacting πN system as a particle of continuous mass. In addition to the preceding five rules we have the sixth rule specifically for the thin, directed, rectangular, hatched box is listed below.

(6) Assign an energy $z+\epsilon^{\Delta}$ to such lines. z is the difference between the mass of the πN system and that of a nucleon; $z \geq m_{\pi}$. ϵ^{Δ} is the kinetic energy of the system. If $\vec{P}$ is the total momentum, $\epsilon^{\Delta}=\frac{1}{2}\vec{P}^2/(M+z)$. Also assign a multiplicative weight factor $(1/\pi)\,\mathrm{Im}t(z)$, where $t(z)$ is the πN scattering amplitude for total c.m. energy $W=m+z$. Specifically,

$$\mathrm{Im}t(z)=4\pi \sum_{I,J}^{1/2,3/2} \frac{W}{M} \frac{\eta_{2I,2J}(W)\cos\delta_{2I,2J}(W)-1}{2q^3} \phi(q,k,k')P_{2I,2J}(\alpha,\beta,\vec{k},\vec{k}') , \tag{A1}$$

q being the c.m. momentum for the total energy W. $\alpha(\beta)$ and $\vec{k}(\vec{k}')$ are the initial (final) isospin ($\alpha=1,2,3$) and momentum of the pions. These rules assume that the baryons are nonrelativistic. $P_{2I,2J}$ is the channel projection operator. Thus, in the static approximation

$$P_{33}(\alpha,\beta,\vec{k},\vec{k}')=(\delta_{\alpha\beta}-\tfrac{1}{3}\tau_{\beta}\tau_{\alpha}) \times(3\vec{k}\cdot\vec{k}'-\sigma\cdot\vec{k}'\sigma\cdot\vec{k}) . \tag{A2}$$

The quantity $\phi(q,k,k')$ is a form factor function which relates the full-off-mass shell amplitude to the on-shell amplitude. By definition $\phi(q,k,k')=1$ when $q=k=k'$. The function $\phi(q,k,k')$ is not explicitly written in the expression in the main body of this paper. The momentum integrals were cut off at an upper limit of $10m_{\pi}$, which represents an approximate treatment of the off-shell function ϕ.[5]

[1]H. Garcilazo, Nucl. Phys. A302, 493 (1978); G. Miller and J. E. Spencer, Ann. Phys. (N.Y.). 100, 562 (1976). Also see the review article by A. W. Thomas and R. H. Landau in Phys. Rep. 58, 121 (1980).

[2]M. Ericson and T. E. O. Ericson, Ann. Phys. (N.Y.) 36, 323 (1966).

[3]L. L. Foldy and J. D. Walecka, Ann. Phys. (N.Y.) 54, 447 (1969). For one of the first applications of FSA to the π-nucleus problem, see M. G. Piepho and G. E. Walker, Phys. Rev. C 9, 1352 (1974).

[5]N.-C. Wei and M. K. Banerjee, Phys. Rev. C 22, 2061 (1980).

[6]J. W. Van Orden, S. J. Wallace, M. K. Banerjee, and D. M. Schneider, Phys. Rev. C 23, 2157 (1981).

[7]J. B. Cammarata and M. K. Banerjee, Phys. Rev. C 13, 219 (1976).

[8]B. D. Day, Rev. Mod. Phys. 39, 719 (1967).

[9]R. V. Reid, Ann. Phys. (N.Y.) 50, 411 (1968).

[10]This crossing must be distinguished from the crossing of the pion lines at the endpoints of a hatched box.

[11]For q significantly larger than k_F the three defect functions have no nodes and are all positive.